ently the object of investigations in these laboratories.

Acknowledgment. We thank Dr. G. Fini for assistance and suggestions concerning the high-resolution emission spectra and Prof. L. Moggi and Dr. N. Sabbatini for useful discussions. Financial support from Progetto Finalizzato Chimica Fine e Secondaria of the Italian National Research Council (CNR) and European Communities (Contract ESD-025-I) is gratefully acknowledged.

Registry No. $EuW_{10}O_{36}^{9-}$, 84786-68-5; H_2O, 7732-18-5; D_2O, 7789-20-0.

Contribution from the Laboratoire de Photochimie Générale, ERA au CNRS No. 386, ENSCM, 68093 Mulhouse Cedex, France, Institut de Physique Nucléaire (et IN2P3), Université Claude Bernard Lyon I, 69622 Villeurbanne Cedex, France, and Institut de Chimie Inorganique, Université de Fribourg, CH-1700 Fribourg, Switzerland

Relativistic Calculation of the Electronic Structure and Related Properties of $IrCl_6^{2-}$

ANNICK GOURSOT,*† HENRY CHERMETTE,‡ and CLAUDE DAUL§

Received May 3, 1983

Relativistic MS-Xα calculations have been performed for an $IrCl_6^{2-}$ cluster. Good agreement with experiment is obtained for the photoionization, optical (absorption), and electron spin resonance spectra. The incidence of the relativistic effects is pointed out, and the ability of the numerical wave function is emphasized to describe the magnetic properties. The calculation of these latter properties is based on a corrected ground-state wave function and takes into account admixtures of singly and doubly excited states. Different procedures for the normalization of the wave function (truncated by the scattered-wave method) have been tested in the $\langle r^{-3} \rangle$ integral calculations.

Introduction

The hexachloroiridate complex $IrCl_6^{2-}$ is a well-known outer-sphere oxidant, extensively used in electron-transfer reactions,[1] and both its structure and reactivity have been studied for a long time by many experimental techniques. Photochemical studies[2] have shown that this complex can undergo intramolecular redox reactions after irradiation with a wavelength corresponding to the charge-transfer bands. These electrophilic properties arise from the electronic structure of this d^5 complex. The ground-state (GS) electronic energy levels have been investigated in numerous studies of optical,[3-5] magnetic circular dichroism,[6] and photoelectron spectra[7] of this compound, though uncertainties remain for the assignment of some absorption bands.

The magnetic properties have been largely studied by magnetic susceptibility,[8,9] nuclear quadrupole resonance,[10,11] and electron spin resonance[12-16] measurements. The first observation of superhyperfine coupling (interaction of the unpaired electron spin with ligand nuclear spin) was already reported in 1953,[12] leading to the first unambiguous experimental evidence of the delocalization of the metal d electrons over the whole molecule. Since then, this complex has been of considerable experimental and theoretical interest especially due to the covalent nature of the metal-ligand binding and to the existence of π bonds in addition to the σ bonds.

In spite of this ample experimental information, there is a lack of theoretical studies using molecular orbital (MO) models, except extended Hückel calculations (EH).[5,17] This situation is unfortunate since quantitative theoretical description and interpretations of several properties could be of interest (origin and sign of the Fermi term, main contributions to the hyperfine tensor, etc.).

It is therefore interesting to perform a detailed theoretical investigation of this complex by using the multiple-scattering (MS) Xα-MO method, which has already been shown to give realistic descriptions of various properties of complexes.[18-20] As in the previously reported study of $IrCl_6^{3-}$,[21] the mass-velocity and Darwin relativistic corrections are included self-consistently while the spin-orbit interactions are evaluated by an application of first-order perturbation theory, once self-consistency has been reached.

Table I. Xα Parameters for $IrCl_6^{2-}$

region	sphere radii, au	α exchange parameter
Ir	2.5767	0.69310
Cl	2.5961	0.72325
outer sphere	6.9614	0.71894
intersphere		0.71894

In this paper, we will present the ground-state electronic structure of $IrCl_6^{2-}$ and related properties such as electronic excitations and ionization energies. The quality of the MS-Xα relativistic wave functions will be tested by calculating the hyperfine interaction parameters of both the Ir and Cl atoms in the complex. These parameters are then compared to both experimental values and parameters obtained through nonrelativistic calculations. The great importance of the relativistic corrections, particularly on the Fermi term, which reflects the

† ENSCM.
‡ Université Claude Bernard Lyon I.
§ Université de Fribourg.

(1) (a) Gardner, H. C.; Kochi, J. K. *J. Am. Chem. Soc.* **1975**, *97*, 1855. (b) Chen, J. Y.; Kochi, J. K. *Ibid.* **1977**, *99*, 1450. (c) Wong, C. L.; Kochi, J. K. *Ibid.* **1979**, *101*, 5593.
(2) Balzani, V.; Carassati, V. "Photochemistry of Coordination Compounds"; Academic Press: London, 1970.
(3) Jørgensen, C. K. *Mol. Phys.* **1979**, *2*, 309.
(4) Jørgensen, C. K. *Acta Chem. Scand.* **1963**, *17*, 1034.
(5) Sleight, T. P.; Hare, C. R. *J. Phys. Chem.* **1968**, *72*, 2207.
(6) McCaffery, A. J.; Rowe, M. D.; Rice, D. A. *J. Chem. Soc., Dalton Trans.* **1973**, 1605.
(7) Cox, L. E.; Hercules, D. M. *J. Electron Spectrosc. Relat. Phenom.* **1973**, *1*, 193.
(8) Westland, A. D.; Bhiwandker, N. C. *Can. J. Chem.* **1961**, *39*, 2353.
(9) Sloth, E. N.; Gardner, C. S. *J. Chem. Phys.* **1954**, *22*, 2064.
(10) Ito, K.; Nakamura, D.; Ito, K.; Kubo, M. *Inorg. Chem.* **1963**, *2*, 690.
(11) Lindop, A. J. *J. Phys. C* **1970**, *3*, 1984.
(12) Owen, J.; Stevens, K. W. H. *Nature (London)* **1953**, *171*, 836.
(13) Griffiths, J. H. E.; Owen, J.; Ward, I. M. *Proc. R. Soc. London, Ser. A* **1954**, *219*, 526.
(14) Griffiths, J. H. E.; Owen, J. *Proc. R. Soc. London, Ser. A* **1954**, *226*, 96.
(15) Griffiths, J. H. E.; Owen, J.; Park, J. G.; Partridge, M. F. *Proc. R. Soc. London, Ser. A* **1959**, *250*, 84.
(16) Thornley, J. H. M. *J. Phys. C* **1968**, *1*, 1024.
(17) Cotton, F. A.; Harris, C. B. *Inorg. Chem.* **1967**, *6*, 376.
(18) Goursot, A.; Pénigault, E. *Chem. Phys.* **1981**, *61*, 83.
(19) Weber, J.; Goursot, A.; Pénigault, E.; Ammeter, J. H.; Bachman, J. J. *Am. Chem. Soc.* **1982**, *104*, 1491.
(20) Lebeuze, A.; Makhyoun, M. A.; Lissilour, R.; Chermette, H. *J. Chem. Phys.* **1982**, *76*, 6060.

0020-1669/84/1323-0305$01.50/0

Table II. Ground-State Energy Levels[a] and Charge Distribution of $IrCl_6^{2-}$ in D_{4h} Symmetry

MO ($O_h \rightarrow D_{4h}$)	E, Ry	Ir				Cl_{eq}			Cl_{ax}				
		s	p	d	f	s	p_σ	p_π	s	p_σ	p_π	int	out
$3e_g$ $3b_{1g}$	−0.425			52		1	12		2	21		8	4
$5a_{1g}$				63				26				10	1
$2t_{2g}$ $2b_{2g}$	−0.692			63				14			12	10	1
$3e_g$								88				11	1
$1t_{1g}$ $1a_{2g}$	−0.789							44			44	12	
$2e_g$													
$4t_{1u}$ $5e_u$	−0.824		1		2		48	25			12	10	2
$4a_{2u}$			1		2			52			34	9	2
$1t_{2u}$ $1b_{2u}$	−0.834				1			84				14	1
$4e_u$					1			32			53	14	1
$3t_{1u}$ $3e_u$	−0.921		6				46	18			17	11	2
$3a_{2u}$			6					29			52	11	2
$1t_{2g}$ $1b_{2g}$	−0.975			28				54				17	1
$1e_g$				28				26			28	17	1
$2e_g$ $2b_{1g}$	−1.048			42		2	56						
$4a_{1g}$		1		39		2	36		1	21			
$2a_{1g}$ ($3a_{1g}$)	−1.057	19		3		2	28		2	39		6	1
$2t_{1u}$ $2e_u$	−1.715		2			93						4	1
$2a_{2u}$			2						93			4	1
$1e_g$ $1b_{1g}$	−1.721			5		92						3	
$2a_{1g}$				5		37			54	1		3	
$1a_{1g}$ ($1a_{1g}$)	−1.769	5				52	1		36			5	1
$1t_{1u}$ $1a_{2u}$	−4.292		100										
$1e_u$			100										

[a] The highest occupied level is $2b_{2g}$ ($2t_{2g}$).

electronic spin density of the Ir nucleus, will thus be demonstrated.

Calculation Parameters

The $IrCl_6^{2-}$ anion has been studied experimentally with various counterions and diluted in numerous diamagnetic matrices. The structures of the studied cluster depend strongly on the environment, the $IrCl_6$ octahedron being more or less distorted. However, $(NH_4)_2IrCl_6$ and K_2IrCl_6 have been shown to have regular $IrCl_6$ octahedra.[11,14] To make an easier comparison with all the experimental results, we have thus chosen the O_h symmetry for $IrCl_6$ as determined in K_2IrCl_6 X-ray measurements,[11] with Ir–Cl = 0.231 nm.

In order to compare the present results more easily with those of $IrCl_6^{3-}$ and to split up the orbital multiplets associated with the d–d transitions,[21] we have also performed calculations in D_{4h} symmetry. The values of the MS–Xα parameters are gathered in Table I. The atomic α values are taken from calculations of Schwarz.[22,23] A weighted average of these atomic values is chosen for the interatomic and extramolecular regions (intersphere and outer sphere). The nonempirical procedure of Norman[24] was used to obtain the overlapping atomic sphere radii, which are taken to be 85% of the atomic charge radii calculated from the atomic density superposition. A 18.5% overlapping ratio is then obtained. An externally tangent outer sphere is used in each calculation, which also serves as a "Watson sphere",[25] on which a positive charge is distributed to simulate the stabilizing effect of the environment on the complex anion. All the calculations have been performed with a charge of 3+ on the Watson sphere, in order to shift the energy levels downward and thus to prevent some eigenvalues from becoming too close to zero. Partial waves up to $l = 4$ are included in the multiple-scattering expansions in the iridium sphere and in the extramolecular region and up to $l = 1$ in ligand spheres.

All the calculations of ionization and transition energies have been performed with spin polarization and by using Slater's transition-state formalism,[26] which takes into account second-order relaxation effects.

Results and Discussion

1. Description of the Ground-State Electronic Structure. We do not report here a comparative diagram between nonrelativistic (NR) and relativistic (R) eigenvalues. Indeed, for both core and valence levels, the evolution from NR to R calculations is quite similar to that previously obtained from $IrCl_6^{3-}$,[21] i.e. contraction of s and p orbitals and expansion of d and f orbitals. The calculated spin–orbit parameters are also quite comparable to those reported previously for $IrCl_6^{3-}$. As an example, the ζ_{5d} ($IrCl_6^{2-}$) value is 4900 cm^{-1} for the $2t_{2g}$ MO and 6050 cm^{-1} for the $3e_g$ MO, while the corresponding values are 4700 and 5500 cm^{-1}, respectively, for the Ir(III) complex. As for $IrCl_6^{3-}$, the Ir ζ_{6p} remains constant for all the valence levels, while the metal ζ_{5d}, ζ_{5f}, and ζ_{6s} and the Cl ζ_{3p} are shown to increase with increasing energies.

The electronic energy levels and corresponding charge distributions of the ground-state configuration of $IrCl_6^{2-}$ are reported in Table II. These results have been obtained in a

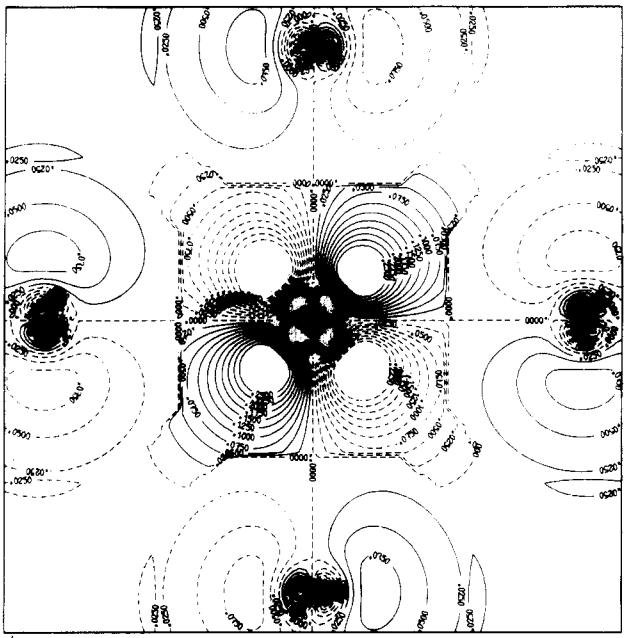

Figure 1. Wave function contours of the $2t_{2g}$ HOMO of $IrCl_6^{2-}$. Positive wave function contours are indicated by a solid line while negative contours are represented by a dashed line. Contour values run from 0 to 0.25 by 0.025 step.

(21) Goursot, A.; Chermette, H. *Chem. Phys.* **1982**, *69*, 329.
(22) Schwarz, K. *Phys. Rev. B: Solid State* **1972**, 2466.
(23) Schwarz, K. *Theor. Chim. Acta* **1974**, *34*, 225.
(24) Norman, J. G., Jr. *J. Chem. Phys.* **1974**, *61*, 4630.
(25) Watson, R. E. *Phys. Rev.* **1958**, *111*, 1108.
(26) Slater, J. C. *Adv. Quantum Chem.* **1972**, *6*, 1.

non-spin-polarized (NSP) calculation. The highest occupied MO (HOMO) is $2t_{2g}$, which accommodates 5e. The HOMO corresponds to nonbonding interactions of the Ir $5d_\pi$ (d_{xz}, d_{yz}, d_{xy}) orbital with the Cl $3p_\pi$ atomic orbitals (AO) (see Figure 1).

Due to an appreciable Cl p_π character, this MO exhibits an important covalent delocalization. If the intersphere charge is fully attributed to the ligands,[18,19] the metal character of the HOMO is 63%. It does not exceed 65% if part of the intersphere is attributed to the metal (see section 5).

The unpaired electron is thus highly delocalized over the whole molecule, each chlorine containing about 6% of this electron. This result is in good agreement with the experimental values of 5.3% or 6.57%, as obtained from ESR or NQR data, respectively.[11,27] From ESR parameters, e.g. g value reduction and ligand hyperfine splitting, Thornley[16] obtained two different evaluations of the electron delocalization (9.3 and 5.3%, respectively).

As a matter of fact, we will see further that the use of our calculated parameters, associated with numerical terms derived from the MS–Xα radial functions, lead to a g value and metal and ligand hyperfine parameters in very good agreement with experiment.

The high covalency of the HOMO was not predicted by the extended Hückel model,[17] which gave a calculated metal character of 85%.

The π-bonding interactions in $IrCl_6^{2-}$ are provided by the $1t_{2g}$ MO, where the metal character amounts to 28%.

Most the of σ covalent metal–ligand interactions occur through the $2e_g$ and $2a_{1g}$ MOs, which correspond to bonding interactions between the Cl $3p_\sigma$ and the Ir $5d_\sigma$ (d_{z^2}, $d_{x^2-y^2}$) and 6s orbitals, respectively. The most striking feature that arises from a comparison between the $IrCl_6^{3-}$ and $IrCl_6^{2-}$ complexes is the increased σ and π covalency for the Ir(IV) complex, correlated to a substantial increase of the π-electron delocalization: the Ir $5d_\pi$ contribution decreases from 78% to 64% for the HOMO and increases from 15% to 28% for the $1t_{2g}$ bonding MO. This result is in agreement with far-infrared measurements,[28,29] which have shown that the metal–chlorine stretching frequency increases with the Ir oxidation number, accompanied by an increase of the covalent character of this bond. Similarly, a comparison of the valence-band intensities in the XPS spectra of both complexes leads to the same conclusion.[7]

The $3t_{1u}$, $1t_{2u}$, and $4t_{1u}$ MOs are typical ligand π type orbitals and are mainly localized in chlorine spheres and in the interatomic region. However, $3t_{1u}$ has a nonnegligible Ir 6p ($\sigma + \pi$) contribution (6%), leading to participation of the metal 6p orbitals to the π bonding, which amounts to 0.21e.

In order to take into account the spin polarization effects for describing all the 1e properties of $IrCl_6^{2-}$, additional calculations have been performed by using the spin-polarized (SP) MS–Xα formalism. For the ground-state electronic structure, the levels with predominant Ir 5d contribution exhibit the largest energy splittings: 0.03 Ry between the $2t_{2g}\downarrow$ (3e) and the $2t_{2g}\uparrow$ (2e), while ligand type levels undergo very small splittings ($\leq$0.003 Ry).

Concerning the composition of the wave functions, the open-shell $2t_{2g}$ electrons are slightly more delocalized in the SP than in the NSP calculation (61% of metal character instead of 63%). As a consequence, it turns out that the Ir 5d contribution of $1t_{2g}$ is larger in SP (31%) than in NSP (28%). These are examples of the largest discrepancies between NSP and SP results. These differences in charge distributions among the MOs do not give rise to any significant changes in the total charge calculations, since slight increases of metal contributions in spin-up MOs are generally compensated by slight decreases in spin-down MOs or vice versa.

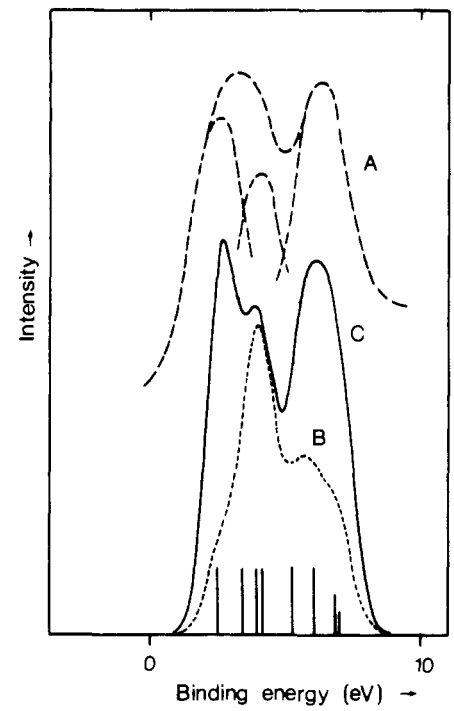

Figure 2. Photoionization spectra of the valence region of $IrCl_6^{2-}$: A, experimental spectrum; B, total density of states; C, theoretical spectrum.

The population analysis is thus performed in the NSP case and leads to the charge distribution

$$Ir^{75.98}[5d^{6.74}(5d_\pi^{4.88}5d_\sigma^{1.86})6s^{0.52}6p^{0.54}5f^{0.18}][Cl^{17.50}]$$

As already mentioned, the interatomic and extramolecular charges are fully attributed to chlorines.

With respect to the ionic model of an Ir^{4+} cation ($5d^5$ configuration), surrounded by six Cl^- anions, the net charge of 1.02+ on the metal results from a transfer of 3.10e from the 3p chlorine orbitals to the metal $5d_{z^2}$, $5d_{x^2-y^2}$, 6s, 6p, and 5f orbitals and a back-bonding transfer of 0.12e from the metal $5d_{xy}$, $5d_{yz}$, and $5d_{xz}$ orbitals to the $3p_\pi$ ligand orbitals.

With respect to $IrCl_6^{3-}$, the σ donation from Cl 3p to Ir $5d_\sigma$ orbitals is substantially enhanced (from 1.56e to 1.86e), while the π back-bonding is decreased from 0.48e to 0.12e.

The removal of a π electron from the $2t_{2g}$ HOMO of $IrCl_6^{3-}$ results in a redistribution of σ and π electrons between metal and ligands, leading to a greater σ and π covalency; the quasi-electroneutrality of the $IrCl_6^{3-}$ charge distribution, namely 0.56e on Ir and –0.59e on each Cl, is not maintained since it becomes 1.02+ and 0.50–, respectively. This 1.02+ calculated net charge on the Ir atom is slightly higher than the 0.90+ value predicted by EH calculations,[17] probably because of the substantially weaker π delocalization of the $2t_{2g}$ HOMO found in this latter work.

The highly positive net charge on the Ir and the strong delocalization of the π electrons in the HOMO are the two main features of the GS electronic structure of $IrCl_6^{2-}$, and both are highly correlated to the electrophilic properties of this outer-sphere oxidant complex.

2. Ionization Energies of $IrCl_6^{2-}$. The experimental photoionization spectrum of the valence region and the MS–Xα ionization energies of $IrCl_6^{2-}$ (NSP calculation) are presented in Figure 2. The calculated values are obtained by using Slater's transition-state procedure,[26] so that the major part of

(27) Cipollini, E.; Owen, J.; Thornley, J. H. M.; Windsor, C. *Proc. Phys. Soc., London* **1962**, *79*, 1083.
(28) Adams, D. M.; Gebbie, H. A. *Spectrochim. Acta* **1963**, *19*, 925.
(29) Clark, R. J. H. *Spectrochim. Acta* **1965**, *21*, 955.
(30) Jørgensen, C. K.; Berthou, H. *Mat.-Fys. Medd.—K. Dan. Vidensk. Selsk.* **1972**, 38 (15).

Table III. Calculated Core Ionization Energies (eV) and Spin–Orbit Splittings of $IrCl_6^{2-}$ Compared with Available Experimental Data

	E_{calcd}	calcd SO splitting	E_{exptl}[a] A	E_{exptl}[a] B	exptl SO splitting
$4f_{7/2}$	72.9		72.0	72.1	
$4f_{5/2}$	76.1	3.2		74.9	2.8
$4d_{5/2}$	297.4			307.4	
$4d_{3/2}$	313.5	16.1		322.4	15.0

[a] Energies shifted by 9.3 eV (case A[7]) or 1.4 eV (case B[30]), so as to bring the first ionization band in agreement with the calculated value.

the orbital relaxation effects is taken into account. The determination of the orbital multiplet structure (state energies) arising in open-shell configurations from the interaction of equivalent electrons goes beyond any 1e model. However, in the present case, the descent in symmetry from O_h to D_{4h} has the advantage of splitting the orbital multiplets ($T_2 \rightarrow B_2 + E$; $T_1 \rightarrow A_2 + E$; $E \rightarrow A_1 + B_1$), and at the same time, SP calculations lead to good approximations of the individual terms of the spin multiplets. This technique allows us to calculate the energies of the multiplet states arising, for example, from the t_{2g}^4 or $t_{2g}^5t_{2u}^5$ configurations. However, in our case, the resolution of the experimental XPS bands is larger than 2 eV for the most resolved ones, so that NSP calculations are sufficient to account for the experimental spectrum, as can be seen in Figure 2. Nevertheless, as an example, the first ionization band structure has been investigated through SP calculations in D_{4h} symmetry including calculation of the spin–orbit (SO) interactions; this is discussed later in this paragraph. The comparison of our calculated energies with the experiment requires a shift in the (experimental) values in order to take into account both the uncertain position of the Fermi level in insulators and the dependence of the theoretical values on the Watson sphere charge (cf. section 1). For core and valence levels, the shifts are done in order to obtain the fit of the experimental and calculated first ionization energies in the valence band (VB). The calculated spectrum, shown with the experimental one in Figure 2, has been obtained by weighting the local densities of states (LDOS) with the Ir 5d, Ir 6s, and Cl 3p atomic photoemission cross sections.[31] The total density of states (DOS), depicted in Figure 1, is obtained by convolution of the weighted calculated ionization energies by a Gaussian (0.6 eV hwhm) relationship. It is worth noting the very good agreement between the calculated and experimental spectra; moreover, a better fit could probably be obtained by use of a slightly different ratio of atomic cross sections, as it is well-known that the atomic photoemission cross section is not totally independent of the oxidation number of the atom (i.e. of the compound in which the atom is involved).

As for $IrCl_6^{3-}$, and supporting the interpretation of Cox et al.,[7] the first ionization band is assigned to the HOMO $2t_{2g}$ and the second one to the set of neighboring nonbonding ligand π MOs ($1t_{2g}$, $4t_{1u}$, $1t_{2u}$). The third experimental band, at highest energy, includes the ionization of four MOs: $3t_{1u}$, with Ir 6p and Cl $3p_\sigma$ and $3p_\pi$; $1t_{2g}$ and $2e_g$, which assume the major π and σ bonding in the complex, respectively; and $2a_{1g}$, with Ir 6s and Cl $3p_\sigma$ contributions. It has to be noted that the separations between the lower energy and higher energy peaks in the VB are very well reproduced by this relativistic calculation, which has induced a 5d-orbital expansion. It leads to a good quantitative description of their evolution from $IrCl_6^{3-}$ to $IrCl_6^{2-}$, particularly the substantial decrease of the separation between the first and second bands, resulting from a greater covalency in the Ir(IV) complex.

The binding energies of the Ir 4d and 4f core levels are compared in Table III with available experimental values. As for $IrCl_6^{3-}$, the calculated SO splittings are in very good agreement with experiment. The $4f_{7/2}$ and $4f_{5/2}$ binding energies are also well reproduced while the $4d_{5/2}$ and $4d_{3/2}$ binding energies are clearly underestimated by the calculations.

Let us now calculate the multiplet structure of the low binding energy band, to see if the interelectronic repulsion and SO effects are responsible for the substantial width of the experimental band (about 2.6 eV). In fact, the MS–Xα ionization energies, which have been presented above, correspond to configuration barycenters. For the first deconvoluted band, the calculated ionization energy corresponds to the barycenter of the four states $^3T_{1g}$, $^1A_{1g}$, ^1E_g, and $^1T_{2g}$ of a t_{2g}^4 configuration.

Moreover, the SO interactions of this Ir complex are expected to be significant, and in fact, the calculated SO parameter ζ_{5d} of iridium has a value of 4900 cm^{-1} for the HOMO. When the SO coupling is taken into account, neglecting the interaction with other configurations, the four t_{2g}^4 excited states are split into a total of seven terms: A_1 ($^3T_1$), E ($^3T_1$), T_2 ($^3T_1$), A_1 ($^1A_1$), E (^1E), and T_2 ($^1T_2$), which are actually to be related with the first ionization band. As explained previously,[21] the use of descent in symmetry from O_h to D_{4h} has the advantage of splitting the orbital multiplets, while the individual terms of spin multiplets are located from spin-polarized calculations.

To obtain the energies of the seven terms above, we will thus proceed in two steps: first, calculate appropriate ionization transition states in D_{4h} symmetry to reach the energies of the four t_{2g} states $^3T_{1g}$, $^1A_{1g}$, ^1E_g, and $^1T_{2g}$ and, then, apply SO coupling by use of perturbation theory. In the first step, SP calculations have been performed, by using the transition-state procedure, to calculate the energies of the states related to the e_g^4, $e_g^3b_{2g}^1$, and $e_g^2b_{2g}^2$ (D_{4h}) configurations, originating from the t_{2g}^4 (O_h) one. The calculated values are 11.97 eV for $^3T_{1g}$ ($^3A_2$, ^3E), 12.25 eV for $^1A_{1g}$ (A_{1g}), and 12.47 eV for ^1E_g ($^1A_{1g}$, $^1B_{1g}$) and $^1T_{2g}$ ($^1B_{2g}$, ^1E_g). One may notice that the last two states have the same calculated energy. This result is in agreement with the equality of the ^1E_g and $^1T_{2g}$ diagonal elements of the electrostatic matrices for the t_{2g}^4 configuration.

The spin–orbit interactions are then introduced by means of a SO coupling matrix of the t_{2g}^4 configuration, which is assumed to depend only upon the effective iridium SO operator ζ_{5d}.[32] This operator is obtained by weighting the ζ_{5d} value for $2t_{2g}$ (4900 cm^{-1}) by the fraction of metal 5d charge in this MO (0.65), leading to an effective value of 3190 cm^{-1}. Accordingly, the energies of the seven states arising from the $2t_{2g}$ ionization are, in increasing order, 11.26, 11.77, 12.00, 12.00, 12.57, 12.64, and 12.64 eV. These values are sufficiently close to induce a single broad experimental band. The convolution of these seven states by 0.6 eV hwhm Guassians do not let any structure appear in the final, almost unskewed peak (let us remember that the best experimental resolution obtained in standard, but monochromatized, ESCA apparatus amounts to 0.6 eV, although the synchrotron radiation source allows a 0.15-eV resolution).

3. Electronic Excitation Energies. As compared to first-row transition-metal complexes, the absorption spectra of the third-row ones exhibit significantly more intense bands in the low-energy region. These bands have been assigned to ligand to metal charge-transfer (LMCT) bands by Jørgensen, who has supplied most of the extensive studies on electron-transfer spectra of polyhalide complexes.[33,36] More recently, magnetic

(31) Scofield, J. H. *J. Electron. Spectrosc. Relat. Phenom.* **1976**, *8*, 123.

(32) Griffith, J. S. "The Theory of Transition-Metal Ions"; University Press: Cambridge, 1961.

(33) Jørgensen, C. K. *Mol. Phys.* **1959**, *2*, 309.

Table IV. Calculated[a] LMCT Electronic Excitation Energies and Experimental Peak Positions of $IrCl_6^{2-}$ (cm^{-1})

transitions[b]		calcd values	exptl peak positions
$E''(^2T_{2g}) \rightarrow U_g'(^2T_{1g})$	FA	18 500	17 300
$\rightarrow E_g'(^2T_{1g})$	FF	19 200	
$E''(^2T_{2g}) \rightarrow U_u'(^2T_{1u})$	AA	21 000	20 400
$E_u'(^2T_{1u})$	AF	22 200	
$E''(^2T_{2g}) \rightarrow E_u''(^2T_{2u})$	AA	23 400	23 200
$\rightarrow U_u'(^2T_{2u})$	AA	24 000	23 800
$E''(^2T_{2g}) \rightarrow U_u'(^2T_{1u})$	AA	30 900	≈32 000
$\rightarrow E_u'(^2T_{1u})$	AF	33 900	
$E''(^2T_{2g}) \rightarrow [1t_{1g}^5 2t_{2g}^5 3e_g^1]$[c]	F	43 000	≈43 100
$E''(^2T_{2g}) \rightarrow [4t_{1u}^5 2t_{2g}^5 3e_g^1]$[c]	A	43 900	
$E''(^2T_{2g}) \rightarrow [3t_{1u}^5 2t_{2g}^5 3e_g^1]$[c]	A	46 400	

[a] SP calculations. [b] Key: A, allowed; F, forbidden. Column 1, Laporte; column 2, symmetry selection rules. [c] Average energy over the LMCT states related to this configuration.

circular dichroism and absorption spectra of $IrCl_6^{2-}$ at room or liquid-nitrogen temperature have been measured, leading to new interpretations of the low-energy LMCT bands.[5,6] A precise assignment of all the excited states responsible for the absorption spectrum of $IrCl_6^{2-}$ is hardly possible, due to the low resolution of the experimental bands and the large number of states rising from all the excited configurations.

As already mentioned above, it is generally not possible to calculate all the states involved in a particular transition since the Xα model provides weighted averages of the excitation energies between two configuration barycenters.

However, a previous work[21] has shown that the use of a descent in symmetry, connected to SP calculations, allows us to split up partially open-shell configurations into individual states. In some cases, like $t_{2g}^5 e_g^1$[21] or t_{2g}^4 configuration (this work) the totality of the states may be calculated. In the present case, the lower symmetry group that has to be used is D_{4h}.

Let us remember that, in the present relativistic calculation, only a one-component wave function is used through the MS-Xα formalism.[21,37,38] Consequently, the SO operator cannot be introduced self-consistently as in relativistic Hartree–Fock–Slater calculations[39,40] or in Dirac–Slater SW-Xα calculations (which use the four components through the MS technique).[41] Therefore, SO effects are taken into account by perturbation theory, once self-consistency has been reached.[21,42] It has been shown on specific examples that this technique is a very good approximation of the Dirac–Slater SW-Xα formalism.[43]

A. LMCT Transitions. The LMCT excited doublet states, resulting from the transfer of 1e from the ligand MOs, $1t_{1g}$, $4t_{1u}$, $1t_{2u}$, and $3t_{1u}$, to the t_{2g}^5 HOMO, are individual, well-separated states. The excited configurations $t_{2g}^6 t_{1g}^5$ and $t_{2g}^6 t_{2u}^5$ would exhibit splittings essentially dependent on the ligand SO parameter $\zeta_{Cl\,3p}$. A simple first-order perturbation calculation is thus sufficient to account for SO interactions.

The $^2T_{2g}$ ground state is split by SO interaction into two levels E_g'' and U_g', lying at $-\zeta_{t_{2g}}$ and $^1/_2\zeta_{t_{2g}}$, respectively. The "true" $IrCl_6^{2-}$ ground state is thus $E_g''(^2T_{2g})$. The LMCT transition energies, obtained from our MS-Xα transition-state calculations, are to be corrected by $\zeta_{t_{2g}}$ and by the SO splittings of the singly excited LMCT states,[36] which are assumed without interaction with the ground state.

Table V. Calculated Ligand Field Excitation Energies and Experimental Peak Positions of $IrCl_6^{2-}$ (cm^{-1})

excited state	calcd value	exptl peak positions	excited state	calcd value	exptl peak positions
$U_g'(^4T_{1g}')$	20 030	20 400[a]	$U_g'(^2T_{1g}'')$	31 600	
$U_g'(^4T_{1g})$	22 500		$E_g'(^2T_{1g})$	32 100	
$U_g'(^4T_{2g}')$	24 700	23 500[a]	$U_g'(^2T_{2g}'')$	32 600	
$E_g'(^4T_{1g})$	25 000		$E_g''(^4T_{2g})$	33 900	
$U_g'(^4T_{2g})$	25 800	24 400[a]	$U_g'(^2T_{1g}')$	34 300	
$E_g'(^4T_{2g})$	26 500		$E_g'(^2A_{1g})$	34 800	
$U_g'(^2T_{2g}')$	26 700	28 000 sh	$E_g'(^2T_{2g})$	36 100	
$E_g''(^4T_{1g})$	29 100		$E_g'(^2T_{1g})$	37 500	
$U_g'(^2E_g'')$	29 100		$U_g'(^2E_g')$	38 900	41 000[a]
$E_g''(^2A_{2g})$	30 900	32 000[a]	$E_g''(^2T_{2g})$	39 300	

[a] Experimental wide band (also) assigned to LMCT transitions; sh = shoulder.

The low-energy spectrum of $IrCl_6^{2-}$ exhibits one weak and two strong bands, the latter being double. Previous work[6,33] assigned the first weak band to the Laporte-forbidden $1t_{1g}$ (Cl π) $\rightarrow$ $2t_{2g}$ transition and the two strong bands to the Laporte-allowed $4t_{1u}$ (Cl π) $\rightarrow$ $2t_{2g}$ and $1t_{2u}$ (Cl π) $\rightarrow$ $2t_{2g}$ transitions, although other authors[5] have attributed the first band to a SO component of $^4T_{1g}$. The calculated LMCT transition energies, which are compared with experiment in Table IV, do support the former assignments.

The SO interactions related to the $^2T_{1g}$ and $^2T_{2u}$ states only involve the calculated SO parameters ζ_{Cl} (835 and 800 cm^{-1}, respectively), leading to relatively weak splittings (≃600 cm^{-1}). This calculated value is in very good agreement with the observed splitting of the peaks at 23 200 and 23 800 cm^{-1}, assigned to the allowed transitions $E''(^2T_{2g}) \rightarrow E_u''(^2T_{2u})$ and $E_g''(^2T_{2g}) \rightarrow U_u'(^2T_{2u})$.

The band located at 20 400 cm^{-1} is assigned to the allowed transition $E_g''(^2T_{2g}) \rightarrow U_u'(^2T_{1u})$. The forbidden transition involving the other SO component $E_u'(^2T_{1u})$ is calculated to occur 1200 cm^{-1} higher in energy, that is, already in the next absorption band. This large SO splitting, also observed for the other $^2T_{1u}$ LMCT state at 32 000 cm^{-1}, is a consequence of the Ir 6p contribution to the t_{1u} MOs, the $\zeta_{Ir\,6p}$ parameter being very large (26 600 cm^{-1}).

The very intense absorption around 43 100 cm^{-1} is assigned to electron-transfer transitions from the ligand MOs $1t_{1g}$, $4t_{1u}$, and $1t_{2u}$ to the LUMO $3e_g$. The calculated values are weighted averages of the energies of all the states involved in the excited configurations.

B. Metal–Metal Transitions. The ligand field transition $2t_{2g} \rightarrow 3e_g$ leads to the excited configuration $t_{2g}^4 e_g^1$, which consists of two quartet and eight doublet terms. From SP calculations, it is possible to estimate only the $^2T_{2g} \rightarrow {}^4T_{1g}$ and $^2T_{2g} \rightarrow {}^4T_{2g}$ transition energies. In spite of the $O_h \rightarrow D_{4h}$ descent in symmetry, the energies of the doublet states cannot be obtained from Xα calculations. We have thus been led to use a ligand field approach and to evaluate the energies of the multiplet terms from the $t_{2g}^4 e_g$ electrostatic matrix, relative to t_{2g}^5, in terms of the Griffith parameters reported in Table VI.

The SO interaction has been taken into account by use of a SO coupling matrix, involving all the states arising from the $t_{2g}^4 e_g^1$ and t_{2g}^5 configuration.[45] This procedure is necessary

(34) Jørgensen, C. K. *Mol. Phys.* **1961**, *4*, 235.
(35) Jørgensen, . K. *Acta Chem. Scand.* **1963**, *17*, 1034.
(36) Jørgensen, C. K. "Halogen Chemistry"; Academic Press: London, 1967; Vol. 1.
(37) Chermette, H.; Goursot, A. In "Local Density Approximations"; Dahl, J. P., Avery, J., Eds.; Academic Press, in press.
(38) Wood, J.; Boring, M. *Phys. Rev.: Condens. Matter* **1978**, *18*, 2701.
(39) Ziegler, T.; Snijders, J. G.; Baerends, E. J. *J. Chem. Phys.* **1981**, *74*, 1271.
(40) Jonkers, G.; De Lange, C. A.; Snijders, J. G. *Chem. Phys.* **1982**, *69*, 109.
(41) Yang, C. *J. Chem. Phys.* **1978**, *68*, 2626.
(42) Boring, M.; Wood, J. H. *J. Chem. Phys.* **1979**, *71*, 32.
(43) Case, D. A.; Yang, C. Y. *J. Chem. Phys.* **1980**, *72*, 3443.
(44) Sambe, H.; Felton, R. H. *Int. J. Quantum Chem.* **1976**, *10*, 155.
(45) Schroeder, K. A. *J. Chem. Phys.* **1962**, *37*, 1587.

Table VI. Parameters Used for the Calculation of the Configuration Interaction Matrix of $IrCl_6^{2-}$

(a) Racah Parameters of Ir[a] (cm^{-1})
$A = 103\,500$ $B = 700$ $C = 2756$

(b) Coulomb and Exchange Integrals of Cl[b] (cm^{-1})
$J_{av} = 76\,200$ $K_{av} = 4620$

(c) Population Parameters[c]
t_{2g}: $n_{Ir} = 0.63$; $n_{Cl} = 0.26$
e_g: $n_{Ir} = 0.52$; $n_{Cl} = 0.36$

(d) One-Electron and Configuration Barycenter Energy Separation[c] (cm^{-1})
$\Delta(\overline{t_{2g}^5} - \overline{t_{2g}^4 e_g}) = 29\,300$ $\Delta(e_g - t_{2g}) = 51\,300$

(e) Griffith's Parameters of Electrostatic Repulsion (cm^{-1})

$a = 58\,579$	$e = 47\,876$	$h = 211.3$
$b = 54\,263$	$f = 2093$	$i = 437.2$
$c = 671.8$	$g = 1222$	$j = 1966$
$d = 48\,886$		

(f) Spin-Orbit Coupling Constants[c] (cm^{-1})
$\zeta_{Ir\,5d} = 4900$ $\zeta_{Cl\,3p} = 590$

(g) Reduced One-Electron Spin-Orbit Coupling Matrix Elements (cm^{-1})
$\langle t_{2g}\|H_{so}\|t_{2g}\rangle = 9267$ $\langle e_g\|H_{so}\|t_{2g}\rangle = 11\,900$

[a] On the basis of the double-ζ wave function of neutral Ir.[58] The obtained values have been reduced as usual by 20% to account for correlation effects. [b] Average of the calculated integrals of neutral Cl with use of Hartree–Fock 2p functions and multiplied by 0.8 to account for electron correlation. [c] Obtained from the reported MS-Xα results.

when SO interactions are expected to be large (as for the Ir 5d element) and for closely spaced states.

The two quartets and eight doublets are thus split into a total of 20 terms. The elements of the SO coupling matrix are expressed in terms of a SO parameter $\zeta = 3190$ cm^{-1}, which is calculated as a weighted average of the effective SO parameters $\zeta_{t_{2g}}$ and ζ_{e_g}.

The 20 calculated ligand field states are spread along the whole spectrum from 20 000 to 39 000 cm^{-1} and are partly hidden under the more intense LMCT bands; they are presented in Table V.

However, according to our results, the weak absorptions near 28 000 and 33 000 cm^{-1} [33] are to be related to closely lying SO components of doublet states. The latter band, observed as a shoulder of the strong absorption at 43 100 cm^{-1}, has also been assigned to the LMCT $3t_{1u} \rightarrow 2t_{2g}$ transition (see above). Our calculations show that the lowest SO component of the lowest quartet U_g' ($^4T_{1g}$) is located near 20 000 cm^{-1}, which is clearly higher than the first calculated LMCT state U_g' ($^2T_{1g}$).

These results indicate that the first weak band of the spectrum, located at 17 300 cm^{-1}, cannot be assigned to the lowest SO component of a quartet state, contrary to some previous assignment,[5] but to the Laporte-forbidden $1t_{1g} \rightarrow 2t_{2g}$ transition, in agreement with other works[6,33] (see above).

4. Characteristics of the MS–Xα Wave Functions. Within the muffin-tin approximation, the MS–Xα 1e wave functions in the atomic spheres are expanded in central field functions

$$\psi(\vec{r}) = \sum_{l,m} C_{l,m}^{A}\, R_l^{A}(r)\, Y_{l,m}(\theta,\Phi) \qquad 0 < r < b_A \qquad (1)$$

where r, θ, and Φ are spherical coordinates referring to the center A, $C_{l,m}^{A}$ is a partial-wave coefficient, $Y_{l,m}$ is a real spherical harmonic, and b_A is the radius of the sphere A. $R_l^{A}(r)$ is the radial wave function, obtained by numerical integration of the radial Schrödinger equation. This procedure allows us to avoid the selection of a LCAO basis set and provides the atomic orbitals of a given l value with a full radial flexibility.

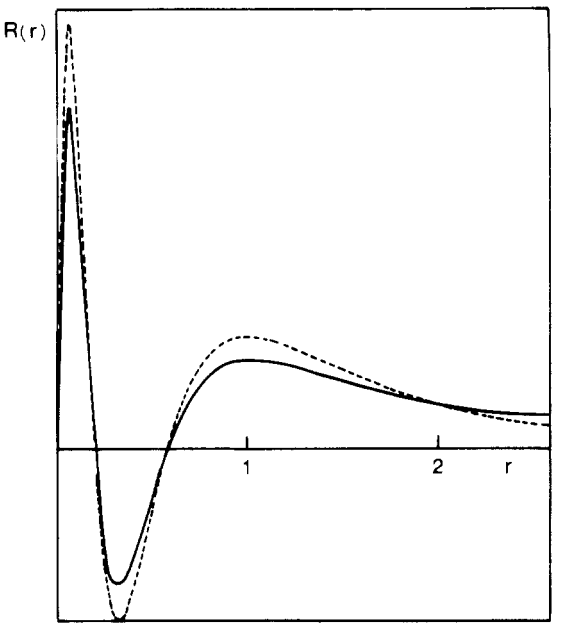

Figure 3. Calculated 5d radial functions in the iridium sphere: straight line, $1t_{2g}$ and $2e_g$ bonding Ir 5d components (almost superposed); dashed line, $2t_{2g}$ (nonbonding) and atomic (Herman–Skillman) Ir 5d orbitals (almost superposed).

For core levels, the wave functions are totally localized inside the (corresponding) atomic spheres, and the normalization is simply given by

$$4\pi \int_0^{b_A} r^2\, R^2(r)\, dr = 1 \qquad (2)$$

For the other (valence + virtual) MOs, the normalization also has to take into account the "scattered waves" in the intersphere region and, obviously, all the atomic orbitals involved in the irreducible representation (for details, see the reviews of Johnson[46] or Rösch[47]). Some Ir 5d radial wave functions $R(r)$ (limited to the atomic sphere) are plotted in Figure 3: one can see the differences between the Ir 5d components of the $2e_g$ (σ bonding), $1t_{2g}$ (π bonding), and $2t_{2g}$ (π nonbonding) MOs. For sake of comparison, the atomic Ir 5d radial wave function, calculated according to Herman and Skillman's procedure[48] and with the same α value, is also reported.

The nonbonding $2t_{2g}$ behaves like the Ir 5d atomic orbital, while the two bonding MOs are clearly more expanded, with less sharp extrema. To compute 1e properties depending only on specific radial functions, it is necessary to renormalize them. Several procedures have been developed, none of them being undoubtedly the best (see section 5):

(1) The radial components can be renormalized within the atomic sphere, neglecting the influence of the tail of the radial function outside the sphere. This approximation is surprisingly quite satisfying since the electrons of the interatomic region have not a well-defined atomic-like character.

(2) The radial basis functions can be extrapolated by using spherical Bessel functions appropriate to the relative values of the constant potential and the wave function eigenvalue. For each wave function, the intersphere charge is distributed among the radial functions, according to an algorithm developed by Case and Karplus.[49] The extension of the radial function has to be sufficiently outside the sphere boundary in

(46) Johnson, K. H. *Adv. Quantum Chem.* **1973**, *7*, 147.
(47) Rösch, N. "Electrons in Finite and Infinite Structures"; Phariseau P., Ed.; Plenum Press: New York, 1977.
(48) Herman, F.; Skillman, S. "Atomic Structure Calculations"; Prentice-Hall: Englewood Cliffs, NJ, 1963.
(49) Case, D.; Karplus, M. *Chem. Phys. Lett.* **1976**, *39*, 33.

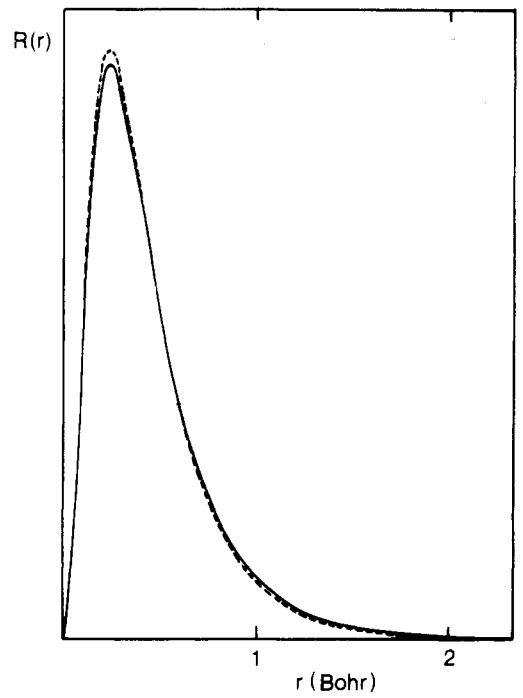

Figure 4. Relativistic and nonrelativistic Ir 4f radial wave functions: straight line, relativistic; dashed line, nonrelativistic.

order to accommodate this additional charge. In some cases, the wave function, although extended to infinity, can accept only a part of the expected charge originating from the intersphere redistribution.

(3) The radial wave function can be extrapolated through an atomic numerical radial function of Herman and Skillman's type.

In both cases 2 and 3, the continuity of the wave function at the sphere boundary is ensured, but not that of its derivative. The incidence of the extrapolation scheme on the calculated magnetic properties is discussed in section 5.

Finally, let us remember that the effects of the self-consistent relativistic corrections (mass–velocity + Darwin terms) on the shape of the radial wave functions of 5d elements have been discussed separately.[50] The contraction of s and p orbitals has been underlined while, on the contrary, the d and f orbitals have been shown destabilized by the self-consistent corrections. As an example, the Ir 4f radial wave function is plotted in Figure 4.

5. Magnetic Properties of $IrCl_6^{2-}$. In a strong crystal field model, the GS configuration of $IrCl_6^{2-}$ is low-spin t_{2g}^5, if interaction with excited configurations is neglected. The GS is thus a Kramers doublet whose properties can be described by a spin Hamiltonian, with a fictitious spin of $^1/_2$.

In the MO approach, the paramagnetic electron moving in the electrostatic potential field of the ligands is not considered as localized on the central ion. The covalency is generally introduced through a covalency parameter leading to a reduction of the orbital contribution to the magnetic moment.[55] The spin–orbit coupling parameter and the expectation values of $\langle r^{-3} \rangle$ used in the description of the hyperfine interaction of the unpaired electron with the Ir nucleus are effectively reduced, while a ligand hyperfine structure appears in addition to the central ion one. Moreover, spin–orbit coupling and electrostatic interactions admix some excited configurations into the GS and provide substantial contributions to the g value and the hyperfine parameters.[16] It is thus worthwhile to determine a corrected GS wave function, in order to evaluate more precisely the g factor and the hyperfine structure constants.

A. Determination of the Corrected GS Wave Function. It has been apparent for many years now that a physically realistic description of the ground state and of the excited states of transition-metal complexes ought to take into account the fact that the involved orbitals are not simply atomic in character, or even atomic orbitals perturbed by their environment, but molecular orbitals made up of contributions from both metal and ligand wave functions.

Recently, one of us derived a method for the calculation of matrix elements of the molecular interelectronic repulsion and spin–orbit operators, for molecules of octahedral or tetrahedral symmetry, over molecular orbital wave functions transforming as e and t_2.[51-54] These elements are parameterized with a set of approximations akin to neglect of diatomic differential overlap. Thus, we have used this method in order to calculate the admixtures of excited ligand field states to the t_{2g}^5 ($^2T_{2g}$) ground state, due to spin–orbit coupling and electrostatic repulsion. The terms that are admixed via spin–orbit coupling are $t_{2g}^4e_g^2A_2$, $t_{2g}^4(^3T_{1g})e_g^2T_{2g}'$, $t_{2g}^4(^1T_{2g})e_g^2T_{2g}''$, $t_{2g}^4e_g^4T_{1g}$, and $t_{2g}^4e_g^4T_{2g}$. The excited terms that are involved in electrostatic admixtures are $^2T_{2g}$ from the following configurations: $t_{2g}^4(^3T_{1g})e_g$, $t_{2g}^4(^1T_{2g})e_g$, $t_{2g}^3(^2T_{1g})e_g^2(^3A_{2g})$, $t_{2g}^3(^2T_{1g})e_g^2(^1E_g)$, $t_{2g}^3(^2T_{2g})e_g^2(^1A_{1g})$, and $t_{2g}^3(^2T_{2g})e_g^2(^1E_g)$.

The configuration interaction matrix of the ground state with all these excited states is calculated by using the model we mentioned above and is then diagonalized. The parameters used in this calculation are given in Table VI, and the corrected ground-state wave function is

$$|+\rangle = C_0[(^2/_3)^{1/2}|^2T_2, -^1/_2, 1\rangle - (^1/_3)^{1/2}|^2T_2, ^1/_2, 0\rangle] + C_1|^2A_2, ^1/_2, a_2\rangle + C_2[(^2/_3)^{1/2}|^2T_2', -^1/_2, 1\rangle - (^1/_3)^{1/2}|^2T_2', ^1/_2, 0\rangle] + C_3[-(^2/_3)^{1/2}|^2T_2'', -^1/_2, 1\rangle + (^1/_3)^{1/2}|^2T_2'', ^1/_2, 0\rangle] + C_4[-(^1/_3)^{1/2}|^4T_1, -^3/_2, 0\rangle - (^1/_2)^{1/2}|^4T_1, -^1/_2, -1\rangle + (^1/_6)^{1/2}|^4T_1, ^3/_2, 1\rangle] + C_5[(^1/_3)^{1/2}|^4T_1, ^1/_2, 0\rangle - (^1/_6)^{1/2}|^4T_2, -^1/_2, 1\rangle - (^1/_2)^{1/2}|^4T_2, ^1/_2, -1\rangle] + \text{negligible contributions from doubly excited states}$$

where $C_0 = 1$, $C_1 = 0.0930$, $C_2 = 0.0130$, $C_3 = 0.0922$, $C_4 = 0.1836$, and $C_5 = 0.0550$. This function is suitable for the calculations of the ESR parameters.

B. The g Tensor. After reduction of the orbital moment, the approximate g value is given to zeroth order by[16,55] eq 3,

$$\bar{g} = -\frac{4k_{\pi\pi} + 2}{3} \tag{3}$$

where $k_{\pi\pi}$ is the orbital reduction factor for the π t_{2g} HOMO. In the LCAO formalism, the $2t_{2g}$ HOMO is described by eq 4, where cp stands for cyclic permutation, $|\Phi_L^{\pi}\rangle$ is one linear

$$|d_{t_{2g}}, xy\rangle = C_M^{\pi}|d_{xy}\rangle - C_L^{\pi}|\Phi_L^{\pi}\rangle \text{cp} \tag{4}$$

combination of four ligand p functions, and $|d_{t_{2g}}, xy\rangle$ is one normalized partner of $2t_{2g}$. The reduction factor has been determined by Stevens[55] (eq 5). It is usual to set $f_P = (C_L^{\pi})^2$

$$k_{\pi\pi} = 1 - 2(C_L^{\pi})^2 \tag{5}$$

so that $k_{\pi\pi} = 1 - 2f_{\pi}$. However, it is confusing that the symbol f_{π} is commonly used for two purposes, namely as the parameter used to define the k reduction factors and also as the actual amount of unpaired spin on the ligands.

For $IrCl_6^{2-}$, t_{2g}^5, the fraction of unpaired spin on each chlorine, is not given by f_{π} but by $^2/_3f_{\pi}$ in order to account

(50) Chermette, H.; Pertosa, P.; Goursot, A.; Pénigault, E., *Int. J. Quantum Chem., Quantum Chem. Symp.* **1983**, *No. 23*, 45g.
(51) Daul, C. Thèse d'aggregation, Université de Fribourg, 1981.
(52) Daul, C.; Day, P. *Mol. Phys.* **1977**, *34*, 1707.
(53) Daul, C.; Weber, J. *Mol. Phys.* **1980**, *39*, 1001.
(54) Daul, C.; Weber, J. *Helv. Chim. Acta* **1982**, *65*, 2486.
(55) Stevens, K. W. H. *Proc. R. Soc. London, Ser. A* **1953**, *219*, 542.

for the three partners of the t_{2g} MO. C_M^{π} and C_L^{π} have been evaluated from the metal (ρ_M) and ligand (ρ_L) MS-Xα charges although these contributions correspond to a gross, rather than to a net, Mulliken atomic population. As a matter of fact, this assumption is not too severe for $2t_{2g}$ since the nonbonding character of this MO allows us to neglect the metal–ligand overlap population.

The major difficulty resides in the assignment of the interatomic charge somehow to the various atoms of the complex. Recently, an unambiguous criterion has been proposed to perform the redistribution of the intersphere charge among the basis functions centered on the atomic spheres.[56] Previously, we had suggested to fully attribute the intersphere charge to the ligands.[19] As a matter of fact, in the case of $IrCl_6^{2-}$ (D_{4h}), we shall see further that for b_{2g} and e_g MOs, the shape of the Ir 5d radial function is such that an extrapolation of the wave function cannot provide a sufficient increase of charge. For the open-shell MO, the greatest possible additional contribution to the metal population is 2%, leading to a negligible decrease of the previously defined electron delocalization. Accordingly, in order to make all the following results consistent, we will take $\rho_L = 1 - \rho_M$ with $\rho_M = 0.65$ deduced from the NSP MS-Xα results. Consequently, we obtain $k_{\pi\pi} = 0.825$, and the zeroth order g value becomes $g = -1.767$.

Thornley[16] has shown that admixtures of states stemming from the singly excited configuration $t_{2g}^4e_g^1$ to the ground state, via spin–orbit and electrostatic interactions, lead to substantial corrections of the zero-order g value.

The corrected GS wave function described above has thus been used to evaluate the additional contributions to the g factor. In terms of the wave function coefficients C_1, C_2, and C_3, the expression for g becomes

$$g = -\frac{4k_{\pi\pi} + 2}{3} - 4k_{\sigma\pi}(\sqrt{2/3}C_1 + (2/3)^{1/2}C_3) - \frac{8k_{ab}\zeta_{ab}}{3E_c} \quad (6)$$

As for $k_{\pi\pi}$, the reduction parameters $k_{\sigma\pi}$ (0.388) and k_{ab} (0.201) have been calculated by using the MS-Xα charges to approximate the net Mulliken atomic populations. Average values of the calculated SO parameters for $1t_{2g}$, $2t_{2g}$, and $3e_g$ have been used to determine the effective SO constants $\zeta_{\sigma\pi}$ (coupling between $2t_{2g}$ and $3e_g$) and ζ_{ab} (coupling between $1t_{2g}$ and $2t_{2g}$); i.e. $\zeta_{\sigma\pi} = 2900$ cm^{-1} and $\zeta_{ab} = 1400$ cm^{-1}. The calculated MS-Xα value of $E_c = 32\,000$ cm^{-1} has been retained for charge-transfer transition energy $\pi(t_{2g}\ (1t_{2g})) \rightarrow d(t_{2g}\ (2t_{2g}))$.

We thus evaluate to −0.011 the additional contributions to the zero-order g value, which leads to a definitive g value of −1.778, in very good agreement with the experimental result (−1.786) for the pure octahedral $(NH_4)_2IrCl_6$ salt. For a comparison with experiment, see Table X.

C. Hyperfine Structure. The ESR spectrum of $(NH_4)_2IrCl_6$[14] exhibits a resolved structure of four hyperfine lines from the Ir nucleus, each of them being split into seven components by a pair of two equivalent Cl nuclei. The experimental values of the hyperfine structure constants are[14,16] $|A| = |B| = (26.3 \pm 0.6) \times 10^{-4}$ cm^{-1} for Ir and $|A\uparrow| = |B\uparrow| = (8.7 \pm 0.15) \times 10^{-4}$ cm^{-1} for Cl. As previously described,[19] the NSP and SP formalism of MS-Xα allows us to calculate with very good accuracy both the isotropic and anisotropic parts of the hyperfine tensor. The isotropic or Fermi contact term, resulting from the polarization of the MOs having s type components in the sphere of the considered atom, is calculated through SP calculations

$$A_F = (8\pi/3)g_e\beta g_N\beta_N[\rho^{\uparrow}(0) - \rho^{\downarrow}(0)] \quad (7)$$

$\rho^{\uparrow}(0)$ and $\rho^{\downarrow}(0)$ being the spin-up and spin-down electronic densities at the nucleus.

A very good estimate[19] of the zero-order anisotropic radial contribution (labeled P_0 for metal and P_0' for ligand) to the hyperfine tensor is obtained from NSP MS-Xα calculations as

$$P_0 = g_e\beta_e g_N\beta_N\rho^{\pi}\langle r^{-3}\rangle \quad (8)$$

where $\langle r^{-3}\rangle$ is the expectation value calculated over the metal $5d_{\pi}$ or ligand $3p_{\pi}$ component of the open-shell MO and ρ^{π} is the metal or ligand MS-Xα charge distribution originating from this MO.

In order to include polarization effects in all the MOs contributing to the anisotropic parameter, it is necessary to perform SP calculations for each irreductible representation Γ, giving the expression

$$P(\Gamma) = g_e\beta_e g_N\beta_N \sum_{k\in\Gamma}[n_k^{\uparrow}\ \rho_k^{\uparrow}\langle r^{-3}\rangle_k - n_k^{\downarrow}\ \rho_k^{\downarrow}\langle r^{-3}\rangle_k] \quad (9)$$

where $n_k^{\uparrow,\downarrow}$ is the occupation number of the $k^{\uparrow,\downarrow}$ MO, $\rho_k^{\uparrow,\downarrow}$ is the gross p or d metal population (or p ligand population) of this MO, and $\langle r^{-3}\rangle_k^{\uparrow,\downarrow}$ is the radial expectation value calculated for this MO.

Suitable combinations of $P(\Gamma)$ according to the various angular factors lead to the determination of the anisotropic hyperfine parameters.

We have performed this calculation for the metal anisotropic parameter P, according to the expression (in D_{4h} symmetry)

$$P = P(A_{1g}) - P(B_{1g}) - P(B_{2g}) + 0.5P(E_g) + 1.4[P(A_{2u}) - 0.5P(E_u)] \quad (10)$$

the unpaired electron being located in b_{2g}.

To obtain P and P' expressed in the commonly used units of 10^{-4} cm^{-1}, and since $\langle r^{-3}\rangle$ is expressed in au^{-3}, the $g_e\beta_e g_N\beta_N$ constant is 3.531 for the Ir nucleus[57] and 16.668 for the Cl nucleus.[16] The nuclear gyromagnetic factors of both Ir and Cl atoms have been weighted and averaged according to the isotopic abundances of these elements.

The radial expectation value of $\langle r^{-3}\rangle$ has been calculated according to

$$\langle r^{-3}\rangle_{nl} = \int_0^b r^{-3}r^2R_{nl}^2(r)\ dr \Big/ \int_0^b R_{nl}^2(r)\ r^2\ dr \quad (11)$$

It is worthwhile to point out here the incidence of the integration boundary b on P values: test calculations have been performed for the metal anisotropic parameter by using the three schemes reported in section 4.

(1) $b = b_{Ir}^0$: Truncation occurs at the sphere boundary. ρ_k is the classical MS-Xα charge in the Ir sphere.

(2) $b = b_{Ir}$: Expansion through spherical Bessel functions such as b_{Ir} accommodates the extra charge arising from the intersphere charge redistribution among the atomic orbitals. When the MOs are much delocalized (b_{2g} and e_g), the Ir sphere cannot be sufficiently swollen to include this additional charge. Two cases have then been considered: (a) the radial wave function expansion is abandoned,[49] i.e. $b_{Ir} \equiv b_{Ir}^0$ (case 1), and (b) the radial wave function is expanded up to the end of the radial mesh (440 points) and the Ir charge ρ_k associated with $\langle r^{-3}\rangle_k$ is taken as including the greatest possible part of the required additional charge.

(3) $b = b_{Ir}$: Expansion occurs through a function of the Herman and Skillman type (440 points), and ρ_k is calculated as in case 2b.

From examination of Table VII, it is obvious that, whatever the type of expansion, both the SP and NSP calculations

(56) Cook, M.; Karplus, M. *J. Chem. Phys.* **1980**, *72*, 7.

(57) Goodman, B. A.; Raynor, J. B. *J. Inorg. Nucl. Chem.* **1970**, *32*, 3406.

(58) Basch, H.; Gray, H. B. *Theor. Chim. Acta* **1966**, *4*, 367.

Table VII. Effects of the Radial Function Truncation on the Anisotropic Parameter P and on the Hyperfine Tensor A for the Ir Nucleus

	NSP results		SP results	
case	P_0[a]	A_0[a,b]	P[a]	A[a,b]
1	29.993	25.80	31.035	26.97
2a			30.805	26.77
2b	29.993	25.80	30.844	26.80
3			30.730	26.70

[a] In 10^{-4} cm^{-1} units. [b] Including correction terms.

performed with expanded radial functions lead to very similar P and A values. The same conclusion is drawn from test calculations on the ligand anisotropic parameter, making us confident in the validity of the expansion procedure.

Indeed, the values obtained in case 1 are not very different from the others, owing to the high degree of localization of the $\langle r^{-3} \rangle$ integrant inside the atomic spheres. The slight differences obtained (<1%) arise from the normalization integrals, which are obviously smaller for truncated functions.

If not specified, the expansion procedure of case 2b has been retained in all the following calculations.

i. Metal Hyperfine Structure. Before comparing the calculated hyperfine structure with experiment, it is worthwhile to examine in detail the different contributions to P and A_F. The values of $P(\Gamma)$ are presented in Table VIII according to the different metal contributions.

As expected from a previous work,[19] it is seen that the polarization effects are large in the valence shell, especially for the 5d and 5p components. The positive values of $P_{5d}(\Gamma)$ arise from the larger expectation values $\langle r^{-3} \rangle_{5d}$ of spin-up levels, through an effect of the unpaired $2b_{2g}$ electron that leads to a contraction of the spin-up radial function.

The substantial negative values of $P(A_{2u})$ and $P(E_u)$ are essentially due to the large differences between the spin-up and spin-down expectation values $\langle r^{-3} \rangle_{5p}$.

In spite of substantial polarization effects, the core polarization parameter $W = P/P_0$ remains very close to unity (1.028). However, the incidence on the A value is not negligible (see Table X).

Table IX reports the individual contributions of the various orbitals possessing metal s components to the Fermi contact term A_F of the hyperfine Ir tensor, obtained through relativistic and nonrelativistic calculations.

The resulting spin density at the origin is highly negative in both cases, the relativistic corrections leading however to a 3 times larger Fermi term. This results from the well-known contraction of s orbitals due to relativistic corrections.[50]

The large relativistic effect shown by the resulting spin densities of $3a_{1g}$ and $4a_{1g}$ is essentially due to the substantial differences in the metal 6s contributions to the spin-up and spin-down densities: ($3a_{1g}$) 20%, 0%; ($4a_{1g}$) 17%, 3%. On the other hand, the substantial contribution of the Ir 5s orbital to the spin density, observed in the relativistic calculation, stems from the large delocalization of the Ir 5d orbital onto the ligands, allowing a greater part of the filled Ir 5s orbital to be found inside the Ir 5d orbital.

Taking into account admixtures of excited configurations to the GS, the hyperfine coupling of the Ir nucleus is given by eq 12. The first bracket represents the zero-order term, while the second one describes the additional corrections.

$$A = -2P\left[\frac{4}{7} - \frac{\kappa}{6}\right] - 2P\left[{}^4/_3 C_1 + {}^{16}/_7(^2/_3)^{1/2} C_2 - {}^{16}/_7(^2/_3)^{1/2} C_3 + {}^2/_7(^1/_3)^{1/2} C_4 - {}^2/_7(^1/_3)^{1/2} C_5 + \left(\frac{4}{7} - \frac{\kappa}{6}\right)\frac{2\zeta_{ab}\beta_\pi}{E_C}\right] \quad (12)$$

This equation is equivalent to that given by Thornley,[16] but the contributions from the $t_{2g}{}^4e_g$ states are expressed in terms of the coefficients C_1, ..., C_5 used in our corrected GS wave function (see section 5A).

ζ_{ab} and E_C have the same values as previously reported for the g factor. β_π is taken from the calculated metal contribution to the π-bonding $1t_{2g}$ MO including part of the intersphere charge (0.32). κ is the usual contact parameter $\kappa = -A_F/P$. The large negative value found for A_F (-32.379×10^{-4} cm^{-1}) leads to a positive κ value nearly equal to 1: $\kappa = 1.050$.

As indicated by Thornley,[16] the magnitude of A is increased when the additional corrections (−0.61) are added to the zero-order term (−24.44). However their amount, which represents less than 1% of $2P$, is only one-tenth of what was assumed by this author. Examination of Table X shows that the calculated A value is in good agreement with experiment.

ii. Ligand Hyperfine Interactions. The covalent electron transfer, which leaves a fraction of unpaired spin in a ligand, induces a hyperfine interaction with the chlorine ligand nucleus. The zero-order term of the ligand hyprfine tensor A′ is

$$-{}^2/_5 f_\pi P'\left(\frac{8}{3} - \frac{5\kappa}{3}\right)$$

According to the MS–Xα formalism, the parameter P' (eq 8 and 9) represents already $f_\pi P'$. Since this calculation has been performed in D_{4h} symmetry, the unpaired electron is located in the b_{2g} orbital, which identifies the $t_{2g}|xy\rangle$ component in O_h (eq 4).

The ligand anisotropic parameter has been calculated in an NSP calculation involving the open-shell MO and taking into account the expression of the radial function according to case 2b (see above). It yields $f_\pi P' = 10.275$ in 10^{-4} cm^{-1} units.

The other contributions to the ligand hyperfine structure are the dipolar interaction term $2A_d$ and corrections due to admixtures of excited states. These latter terms have been evaluated by using our calculated admixture coefficients inserted into expressions similar to those given by Thornley.[16] The parameters $f_\pi = {}^1/_4\rho_L{}^\pi$ and $f_\sigma = {}^1/_3\rho_L{}^\sigma$ ($\rho_L{}^\pi$ and $\rho_L{}^\sigma$ are the ligand charge contributions to the HOMO and LUMO, respectively) have been determined from redistribution of the greatest possible part of the intersphere charge. These correction terms bring a substantial contribution to A' since they amount to 2.03×10^{-4} cm^{-1} about 10% of $2P'f_\pi$, while Thornley predicted 9%. In agreement with this author, the major part (70%) of these corrections is found to arise from

Table VIII. Iridium Anisotropic Hyperfine Parameters for $IrCl_6{}^{2-}$ (D_{4h} Symmetry)

symmetry Γ	$P_{5d}(\Gamma)$	$P_{3d+4d}(\Gamma)$	$P_{6p}(\Gamma)$	$P_{5p}(\Gamma)$	$P_{3p+4p}(\Gamma)$	$P(\Gamma)$[a]
A_{1g}	0.477	−0.012				0.465
B_{1g}	0.358	−0.012				0.346
B_{2g}	8.882	−0.012				8.870
E_g	0.128	−0.024				0.104
A_{2u}			0.100	−0.765	−0.096	−0.761
E_u			0.231	−1.525	−0.193	−1.487

[a] $\Sigma P_{nl}(\Gamma)$.

Table IX. Contributions to Fermi Contact Parameter of the Ir Hyperfine Tensor of $IrCl_6^{2-}$ from Relativistic (R) and Nonrelativistic (NR) SP MS-Xα Calculations

		R	NR
orbital	n^a	$\rho^{\uparrow}(0) - \rho^{\downarrow}(0)$, au	$\rho^{\uparrow}(0) - \rho^{\downarrow}(0)$, au
$4a_{1g}$	6	−11.6415	0.1380
$3a_{1g}$	6	12.7316	0.0022
$2a_{1g}$	6	0.0295	0.0187
$1a_{1g}$	6	0.2370	0.0122
5s	5	−2.3203	−0.4522
4s	4	0.1113	0.00
3s	3	−0.0163	−0.0324
2s	2	−0.1889	−0.0360
1s	1	−0.0370	−0.0125
total		−1.0946	−0.3620

[a] Principal quantum number of the metal s component.

Table X. Comparison of Experimental and Calculated g Values and Hyperfine Parameters (Nonrelativistic (NR) and Relativistic (R) Calculations)

	calcd[a]		
	NR	R	exptl[b]
	g Values		
	−1.762	−1.778	−1.786 ± 0.004
	Hyperfine Parameters		
Ir A_F	−10.713	−32.379	
Ir P	29.187	30.844	
Ir A	−30.8	−25.1	$\|A\| = 26.3 \pm 0.60$
Cl A_F'		−0.307	
Cl P'		10.275	
Cl A'		−8.60	$\|A'\| = 8.71 \pm 0.15$

[a] In 10^{-4} cm^{-1} units. [b] From ref 16.

the charge-transfer contribution.

The dipolar interaction between the magnetic moment of the Cl nucleus and those of the Ir electrons is expressed by eq 13, giving a dipolar contribution of 0.22×10^{-4} cm^{-1}.

$$2A_d = 2g_e\beta_e g_N\beta_N R^{-3} \quad (13)$$

Although one can argue that his procedure is somewhat arbitrary, we found it coherent to evaluate A_d taking R equal to the sum of the Ir^{4+} and Cl^- radii, as calculated from the superposition of the Herman–Skillman densities. This procedure is equivalent to the point-charge approximation of a two-center integral. As expected, the polarization effects of the s orbitals are very weak since the resultant spin density $[\rho^{\uparrow}(0) - \rho^{\downarrow}(0)]$ at the Cl nucleus is only −0.0022, giving a small positive contact parameter $\kappa = 0.030$. These results lead to a negative hyperfine parameter $A' = -8.96 \times 10^{-4}$ cm^{-1}, all corrections included. As shown in Table X, this calculated result is in very good agreement with experiment.

Conclusion

The aim of this work, as a part of studies on heavy-atom halides, was to provide a detailed analysis of the numerous electronic observables of the hexachloroiridate(IV) complex.

In addition to providing a very satisfactory interpretation of the photoelectron and of the electronic absorption spectra—including evaluation of spin–orbit effects—the theoretical model gives a quantitative description of the magnetic properties of this complex. The signs of the hyperfine splittings are not determined experimentally. Our results show that in both cases, for iridium and chlorine, the elements of the hyperfine tensors are negative. As expected, the polarization of the MOs having s type components in the iridium sphere is very dependent on the relativistic contraction of the s type metal orbitals. The value of the Fermi contact contribution for the metal is found comparable with that of the anisotropic term, leading to a positive κ contact parameter slightly greater than unity. The very good agreement of all ESR parameters, i.e. g value and both hyperfine tensors, metal and ligand, clearly demonstrates the coherence of the calculated results.

This is certainly due to the realistic MS-Xα evaluations of the isotropic and anisotropic contributions to the hyperfine interactions but also to the present ligand field treatment, which includes delocalized molecular orbitals and configuration interaction with excited configurations. In fact, our ligand field approach shows that, contrary to Thornley's assumption,[16] it is necessary to include admixtures of the terms of the $t_{2g}^4e_g^1$ and $t_{2g}^3e_g^2$ configurations into the ground state.

The neglect of the biexcited configuration leads to a strong overestimation of the correction for electrostatic interaction. When both these excited configurations are admixed to the ground state, the spin–orbit coupling is then found to provide the prevailing corrections.

The interest in combining the ligand field approach with molecular orbital theory has already been outlined. In addition, the present work shows that it is possible to obtain quantitative results for magnetic properties of complexes as far as the theoretical MO model provides all the needed parameters and radial wave functions of good quality.

Acknowledgment. Part of these calculations have been performed at the Centre de Calcul, CNRS, Strasbourg-Cronenbourg, France; financial support of NATO is gratefully acknowledged (Project No. 010.81).

Registry No. Hexachloroiridate(2−), 16918-91-5.